Redox Biology 55 (2022) 102394

Contents lists available at ScienceDirect

Redox Biology

journal homepage: www.elsevier.com/locate/redox

Induction of reactive oxygen species by mechanical stretch drives endothelin production in neonatal pig renal epithelial cells

Ravi Kumar [1], Hitesh Soni [1], Jeremiah M. Afolabi, Praghalathan Kanthakumar, Pratheesh D. Mankuzhy, Samson A. Iwhiwhu, Adebowale Adebiyi [*]

Department of Physiology, College of Medicine, University of Tennessee Health Science Center, Memphis, TN, USA

ARTICLE INFO

Keywords:
Mechanical stretch
Urinary tract obstruction
Hydrogen peroxide
Endothelin converting enzyme
Endothelin
Acute kidney injury
Neonatal pigs

ABSTRACT

Vasoactive endothelin (ET) is generated by ET converting enzyme (ECE)-induced proteolytic processing of pro-molecule big ET to biologically active peptides. H_2O_2 has been shown to increase the expression of ECE1 via transactivation of its promoter. The present study demonstrates that H_2O_2 triggered ECE1-dependent ET1-3 production in neonatal pig proximal tubule (PT) epithelial cells. A uniaxial stretch of PT cells decreased catalase, increased NADPH oxidase (NOX)2 and NOX4, and increased H_2O_2 levels. Stretch also increased cellular ECE1, an effect reversed by EUK-134 (a synthetic superoxide dismutase/catalase mimetic), NOX inhibitor apocynin, and siRNA-mediated knockdown of NOX2 and NOX4. Short-term unilateral ureteral obstruction (UUO), an inducer of renal tubular cell stretch and oxidative stress, increased renal ET1-3 generation and vascular resistance (RVR) in neonatal pigs. Despite removing the obstruction, UUO-induced increase in RVR persisted, resulting in early acute kidney injury (AKI). ET receptor (ET_R)-operated Ca^{2+} entry in renal microvascular smooth muscle (SM) via transient receptor potential channel 3 (TRPC3) channels reduced renal blood flow and increased RVR. Although acute reversible UUO (rUUO) did not change protein expression levels of ET_R and TRPC3 in renal microvessels, inhibition of ECE1, ET_R, and TRPC3 protected against renal hypoperfusion, RVR increase, and early AKI. These data suggest that mechanical stretch-driven oxyradical generation stimulates ET production in neonatal pig renal epithelial cells. ET activates renal microvascular SM TRPC3, leading to persistent vasoconstriction and reduction in renal blood flow. These mechanisms may underlie rUUO-induced renal insufficiency in infants.

1. Introduction

A blockage along the urinary tract from the kidney to the urethra is a significant cause of kidney injury in infants [1–3]. Urinary tract obstruction can occur in infants due to congenital or acquired conditions, including vesicoureteral reflux, ureteropelvic and bladder outlet obstruction, ureterocele, and urinary tract stones [1–3]. Urinary tract obstruction results in hydronephrosis, renal oxidative stress, and a decline in renal vascular, glomerular, and tubular functions that lead to kidney injury [1–3]. Prolonged obstruction may advance to severe renal inflammation, fibrosis, and chronic kidney disease [1–3]. Irreversible obstructive nephropathy is one of the most common causes of pediatric nephrectomy for non-neoplastic conditions [4,5]. Thus, early diagnosis and treatment are critical to preventing renal loss.

Despite the removal of obstruction, steady-state renal blood flow, and GFR decline because of elevated renal vascular resistance (RVR) [6–8]. High RVR in obstructive vasculopathy could be due to increased vasoconstrictor agonists within the kidneys. Urinary obstruction increased kidney endothelin (ET)1 level, suggesting that renal ET1 may contribute to obstructive nephropathy [9–12]. However, several unanswered questions exist on the ET system's pathophysiological mechanisms in neonatal urinary obstruction. There are three distinct ET

Abbreviations: ET, endothelin; H_2O_2, hydrogen peroxide; ROS, reactive oxygen species; UUO, unilateral ureteral obstruction; rUUO, reversible unilateral ureteral obstruction; AKI, acute kidney injury; SMC, smooth muscle cell; RVR, renal vascular resistance; PT, proximal tubules; TRPC3, transient receptor potential channel 3; DAG, diacylglycerol; IP_3, inositol triphosphate; SR, sarcoplasmic reticulum; ECE, endothelin converting enzyme; IHC, Immunohistochemistry; SOC, store-operated Ca^{2+}; ROC, receptor-operated Ca^{2+}; DMEM, Dulbecco's Modified Eagle Medium; FBS, fetal bovine serum; qRT-PCR, quantitative RT-PCR; tRBF, total renal blood flow; MAP, mean arterial pressure; LVGCC, L-type voltage-gated Ca^{2+} channels.

* Corresponding author.
E-mail address: aadebiyi@uthsc.edu (A. Adebiyi).

[1] Equal contribution.

https://doi.org/10.1016/j.redox.2022.102394
Received 13 February 2022; Received in revised form 23 June 2022; Accepted 1 July 2022
Available online 4 July 2022

Table 1
Oligonucleotide primer sequences.

Gene	Sequence	Accession	Length (bp)
	PCR 1		
ECE1	Forward 5′-GCTCCTCACCCAATGCCTTA-3′ Reverse 5′-GGTTCCCGTCCTTGTCATAC-3′	KP411748.1	108
ECE2	Forward 5′-GTGCTGAGTGAGGTGGGAT-3′ Reverse 5′-AGCCAGCAGTAGAGAGACAC-3′	XM_013982249.2	99
ECE3	Forward 5′-TCCTCGGTTCTTCTCTGGTG-3′ Reverse 5′-TTCTCAGAGGCCAGGTAACG-3′	XM_021078895.1	109
ET1	Forward 5′-GCTCCTGCTCTTCCCTGATG-3′ Reverse 5′-GGCTTCCAAGTCCGTATGGG-3′	NM_213882.1	105
ET2	Forward 5′-AGCGGCTGAGGGACATTG-3′ Reverse 5′-GAGCTATCTCTTCCTCCGCC-3′	XM_021096940.1	107
ET3	Forward 5′-AAAGCCAGGAGGCTTTAGACC-3′ Reverse 5′-CTCCCAGAGGCTCCCTAAAG-3′	NM_001098582.2	106
NOX2	Forward 5′-CATGCCTTCGAGTGGTTTGC-3′ Reverse 5′-TCATCCCAGCCAGTGAGGTA-3′	NM_214043.2	110
NOX4	Forward 5′-GGAACGCACTACCAGGATGT-3′ Reverse 5′-CTTCACAAATGTGCGCTGGG-3′	XM_013979249.2	114
18S rRNA	Forward 5′-CGAAAGCATTTGCCAAGAAT-3′ Reverse 5′-AGTCGGCATCGTTTATGGTC-3′	NR_046261.1	102

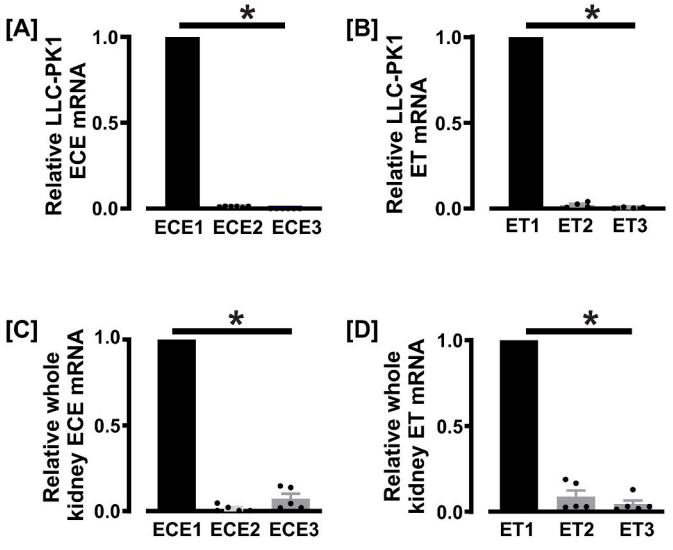

Fig. 1. Relative mRNA expression levels of ECE1-3 and ET1-3 in PT epithelial cells (LLC-PK1) and whole kidneys of neonatal pigs. $P < 0.05$ (one-way ANOVA, with Holm-Sidak post hoc test).

isoforms (ET1, ET2, and ET3) [13,14]. ET2 differs from ET1 by 2 amino acids, whereas ET3 differs by 6 amino acids [13]. Despite their structural similarity, ET isoforms may exhibit distinctive expressions and functions [15,16]. Whether all ET peptides contribute to neonatal obstructive nephropathy is unclear. The molecular links between urinary tract obstruction and elevated ET1 levels are also unknown. Vasoactive ET isoforms are generated by ET converting enzyme (ECE)-induced proteolytic processing of pro-molecule big ET to biologically active peptides. ECE1 is predominantly expressed in tubular regions of the kidneys [17,18]. H_2O_2, a reactive oxygen species (ROS), transactivates the promoter of ECE1 and increases its levels [19]. Urinary obstruction causes significant ROS generation and stretch of renal tubular cells [20–22]. Studies have also shown that mechanical stretch is a potent driver of cellular redox signaling [23–26], but whether renal tubular cell stretch stimulates ROS and downstream ET generation is unresolved.

ET cognate receptors (ET_R) are coupled to G proteins, and their stimulation causes smooth muscle cell (SMC) ion channel activation and ensuing events that control intracellular Ca^{2+} ($[Ca^{2+}]_i$) levels and vascular reactivity [27–29]. Agonist-induced activation of GPCRs stimulates phosphoinositide hydrolysis, resulting in the generation of inositol triphosphate (IP_3) and diacylglycerol (DAG) [30]. Binding of IP_3 to sarcoplasmic reticulum (SR) IP_3 receptors elicits Ca^{2+} release [30–32] which triggers extracellular Ca^{2+} entry via plasma membrane store-operated Ca^{2+} (SOC) channels [30–32]. GPCR stimulation can also cause $[Ca^{2+}]_i$ elevation independently of SR Ca^{2+} via DAG-mediated activation of the receptor-operated Ca^{2+} (ROC) channels [33–35]. The canonical transient receptor potential (TRPC) channels are parts of the molecular components of SOC and ROC [33–35]. Of the 7 members of the TRPC subfamily, only TRPC1, 3, 4, 5, and 6 are expressed in rat renal vessels [36]. Unlike in large arteries, TRPC3 is ~7 times more abundant in resistance size renal microvessels when compared with other TRPC isoforms [36]. ET1 constricts cerebral arteries via activation of smooth muscle cell (SMC) TRPC3 [37], but regional heterogeneity exists in the mechanisms that underlie vasoregulation [38–40]. We have previously shown that TRPC3 mediates ROC entry (ROCE) in neonatal pig renal microvascular SMC, and its expression levels in the kidneys and afferent arterioles are dependent on postnatal maturation [41]. However, despite voluminous work in other vascular beds, the pathophysiology of TRP channels in renal microvascular SMC is poorly understood [42].

Treatments of obstructive nephropathy in rodents have not translated into successful clinical outcomes in humans. Thus, new pathways and animal models are needed to identify early mechanisms of obstructive acute kidney injury (AKI) and new therapeutic targets to prevent renal loss in infants. Rodent sizes limit physiological measurements and interventions in newborns. However, since human and pig renal systems are anatomically and functionally similar, the porcine model may mimic human pathophysiology of obstructive nephropathy more than rodents [43–45]. Mechanical stretch of cultured renal epithelial cells is an in vitro model of unilateral ureteral obstruction (UUO)-induced renal tubular stress [21,46]. The present study used a renal epithelial cell line and short-term UUO model in neonatal pigs to test the hypothesis that stretch-driven ROS generation stimulates ET production in neonatal kidneys, resulting in downstream renal vasoconstriction.

2. Materials and methods

2.1. Animals

All animal experiments were approved by the Institutional Animal Care and Use Committee of the University of Tennessee Health Science Center (UTHSC). The newborn pigs (male; 3–5 days old; approximately 1.5 kg) used in this study were obtained from Nichols Hog Farm (Olive Branch, MS). The experiments followed the NIH and Animal Research guidelines: Reporting of In Vivo Experiments. Animals were randomly assigned to experimental groups. The pigs were anesthetized with ketamine/xylazine (20/2.2 mg/kg; i.m.) and maintained at 37 °C on α-chloralose (50 mg/kg, intravenously) as we have previously described [47–50]. The animals were intubated via tracheostomy and

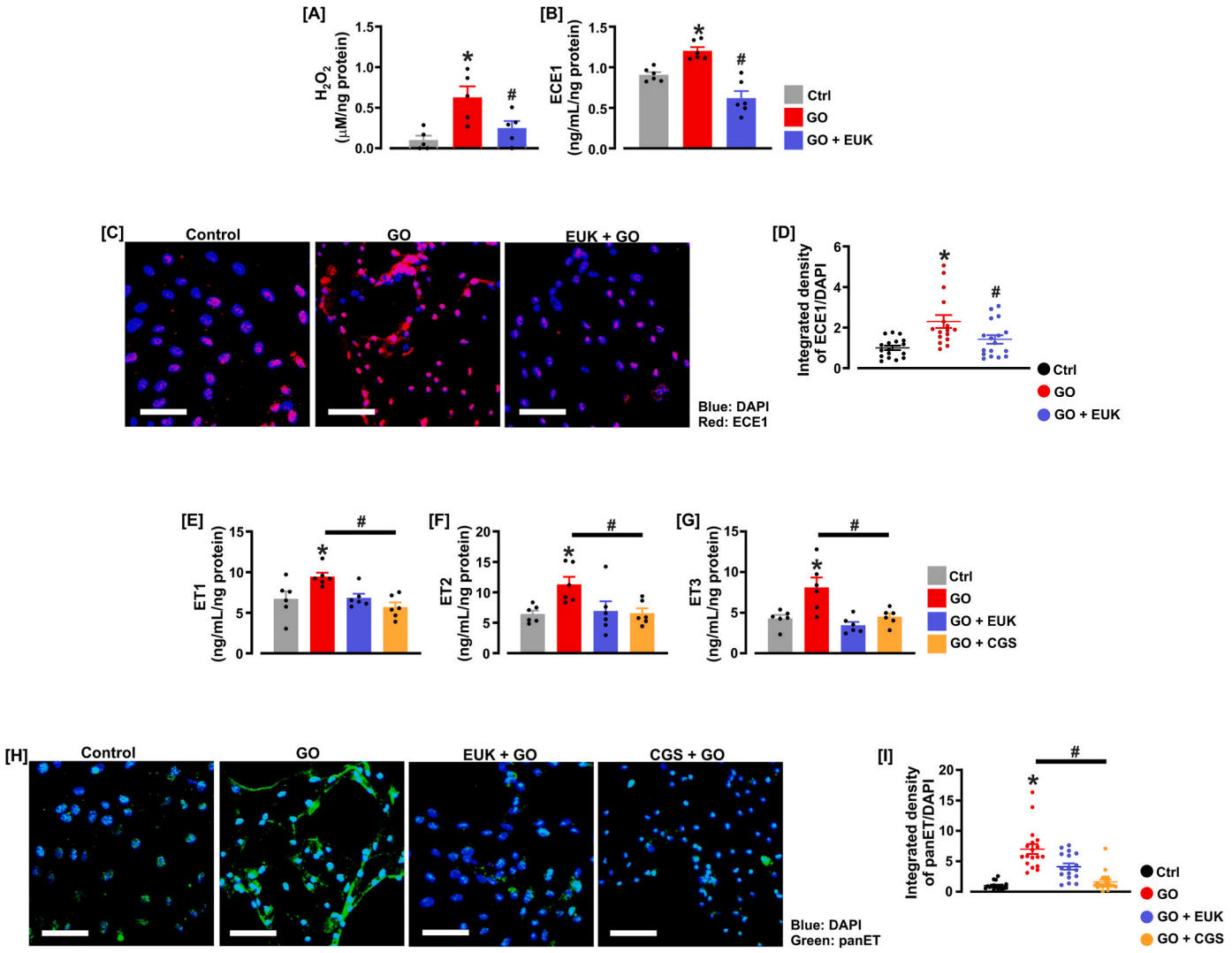

Fig. 2. H_2O_2 generation stimulated ECE1-dependent ET1-3 production by LLC-PK1 cells. A and B, cellular H_2O_2 and ECE1 levels in control, GO (1 U/ml)- and EUK (50 μM) + GO-treated cells. C and D, ECE1 immunostaining in control and GO (1 U/ml)-, and EUK (50 μM) + GO-treated cells. *E*-G, cellular ET1-3 in control, and GO (1 U/ml)-, EUK (50 μM) + GO-, and CGS (10 μM) + GO-treated cells. H and I, panET immunostaining in control and GO (1 U/ml)-, EUK (50 μM) + GO- and CGS (10 μM) + GO-treated cells. *P < 0.05 vs. control; #P < 0.05 vs. GO; (one-way ANOVA, with Holm-Sidak post hoc test). Scale bar = 50 μm.

mechanically ventilated using an infant ventilator (Sechrist Millennium). Arterial blood gas, pH, and hematocrit were measured periodically with a GEM Premier 3000 Blood Gas Analyzer (Instrumentation Laboratory, Bedford, MA). Ventilation was adjusted to maintain PCO_2, PO_2, and pH at physiological ~30 mmHg, > 85 mmHg, and 7.4, respectively.

2.2. LLC-PK1 cell culture

The LLC-PK1 is a porcine kidney epithelial cell line from 3 to 4 weeks old male pigs. The cell line was purchased from the American Type Culture Collection (CL-101; ATCC, Manassas, VA USA). The cells were mycoplasma-free. ATCC routinely uses STR profiling to authenticate their cell lines. The cells were cultured in Dulbecco's Modified Eagle Medium (DMEM) supplemented with 10% (v/v) fetal bovine serum (FBS) and 1% penicillin-streptomycin.

2.3. Mechanical stretch of LLC-PK1

Cultured cells were subjected to 8 h of 10% cyclic uniaxial stretch in a 16-wells single-use flexible silicone plate. The plate was stretched initially for the test cycle, including 5 s stretch, 10 s hold, 10 s recovery, and 5 s rest of 2 repetitions with a ramp magnitude of 1.0 mm. The protocols consist of cycles of 10 s stretch, 10 s hold, 10 s recovery, and with no rest of 980 repetitions with ramp magnitude of 7.0 mm and 1 h holding using software-control MechanoCulture FX Mechanical Stimulation System (CellScale Biomaterials Testing; Waterloo, ON Canada).

2.4. Quantitative RT-PCR (qRT-PCR)

The Direct-zol RNA Miniprep Plus kit (Zymo Research) was used to isolate total RNA. cDNAs were synthesized from the RNA samples with a High-Capacity cDNA Reverse Transcription kit (Life Technologies). qRT-PCR was performed in QuantStudio System using an Applied Biosystems SYBR Green Master Mix kit (Life Technologies). Gene expression levels were normalized to 18S ribosomal RNA as the internal control. The gene-specific oligonucleotide primers used are indicated in Table 1.

2.5. Biochemical assays

Cellular and urine H_2O_2 (K034–H1) levels were determined using the DetectX colorimetric kit (Arbor Assays, Ann Arbor, MI). Urine isoprostane levels were measured with a urinary isoprostane EIA kit (Oxford Biomedical Research, Rochester Hills, MI). Cellular and urine levels

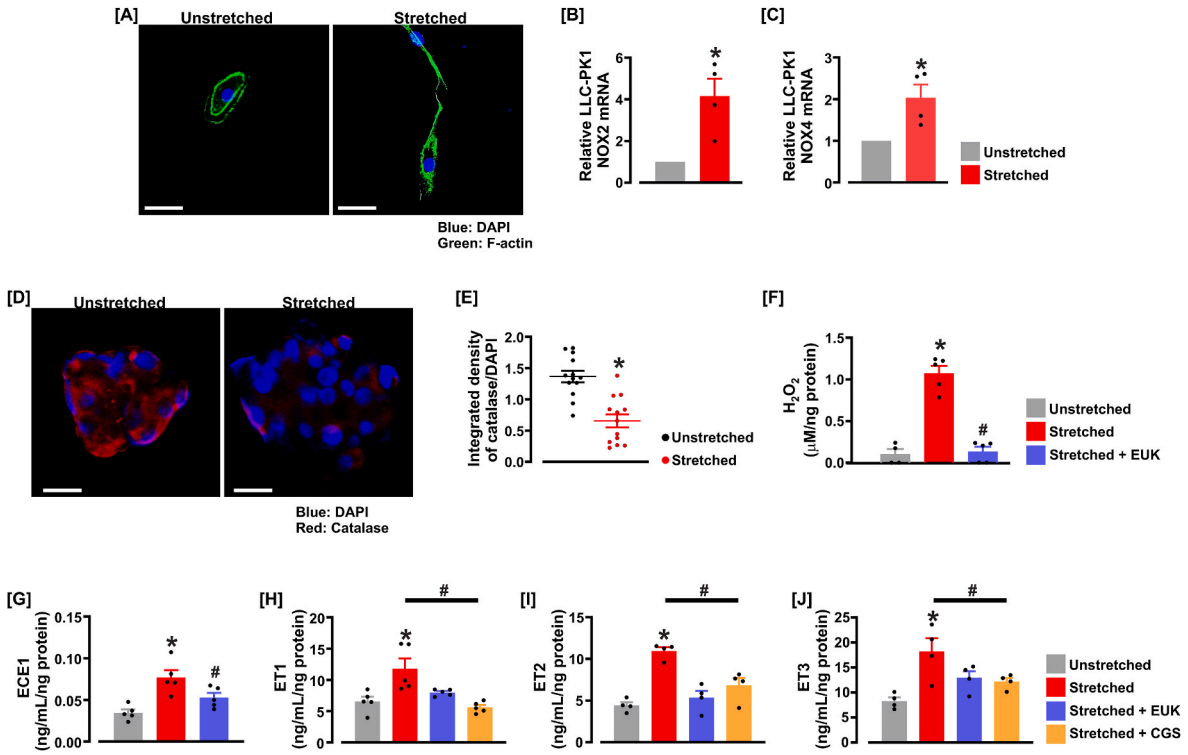

Fig. 3. Mechanical stretch generated H_2O_2 in LLC-PK1 cells and induced ECE1-dependent ET1-3 production. A, F-acting staining in unstretched and stretched LLC-PK1 cells. B and C, relative mRNA expression levels of NOX2 and NOX4 in unstretched and stretched cells. D and E, catalase immunostaining in unstretched and stretched cells. F, cellular H_2O_2 levels in unstretched, stretched, and EUK (50 μM) + stretched cells. G, cellular ECE1 in unstretched, stretched, and EUK + stretched cells. H-J, cellular ET1-3 in unstretched, stretched, EUK + stretched, and CGS + stretched cells. *P < 0.05 vs. unstretched; #P < 0.05 vs. stretched; [unpaired *t*-test (B, C, and E); one-way ANOVA, with Holm-Sidak post hoc test, (F–J)]; Scale bar = 50 μm.

of ECE1 (E0478Po), ET1 (E0230Po), ET2 (E0477Po), and ET3 (E0387Po) were determined using isoform-specific porcine ELISA kits (Bioassay Technology Laboratory, Shanghai, China). Urine lipocalin-2 (NGAL; KIT 044), L-FABP (P1832), and IL-18 (ELP-IL18-1) were quantified with porcine-specific ELISA kits purchased from BioPorto Diagnostic (Hellerup, Denmark), Advanced BioChemicals LLC (Lawrenceville, GA), and RayBiotech (Peachtree Corners, GA), respectively. The kits were used following the manufacturer's instructions. Urinary markers were normalized to urinary creatinine to control for urine flow rate and creatinine clearance variations. Liquid chromatography-tandem mass spectrometry was used to determine creatinine concentrations at the UAB/UCSD O'Brien Core Center for AKI Research at the University of Alabama at Birmingham.

2.6. Histology

Kidney samples were fixed in 4% neutral-buffered formalin, dehydrated in graded alcohols, and embedded in paraffin. The samples were then sectioned for Hematoxylin and Eosin staining. The sections were examined independently by a board-certified veterinary pathologist at TriMetis Life Sciences, Memphis, TN, for morphological damage, including the presence of dilated tubules, protein casts, and infiltration of inflammatory cells. The slides were randomly intermixed and scored blinded: 0 absent, 1+ minimal or rare focal, 2+ mild, 3+ moderate, 4+ marked. Images were taken with a Nikon Ci microscope.

2.7. Immunofluorescence

Cells and kidney sections were fixed with 4% formaldehyde (for about 20 min) and 0.2% Triton X-permeabilized (for about 15 min). The samples were incubated in 5% BSA to block non-specific binding sites and treated overnight at 4 °C with respective primary antibodies. The next day, the samples were washed with PBS and incubated with secondary antibodies for 1 h at room temperature. Following a wash and mount, images were acquired using a Zeiss LSM 710 laser-scanning confocal microscope.

2.8. Immunohistochemistry (IHC)

IHC was blindly performed by IHC World LLC (Ellicott City, MD). The slides were deparaffinized and rehydrated in water. Antigen retrieval was performed using the steam method. Briefly, the slides were steamed in IHC-Tek Epitope Retrieval Solution (IW-1100) for 35 min and then cooled for 20 min. The slides were washed in three changes of PBS for 5 min each and blocked with 3% H_2O_2 for 10 min. After washes, the slides were incubated in primary antibody pan-ET (rat monoclonal) at 1:100 or ECE1 (rabbit polyclonal) at 1:100 diluted with IHC-Tek Antibody Diluent for 1 h at room temperature. The slides were then washed three times in PBS and incubated with biotinylated Rabbit Anti-Rat (for pan-Endothelin) and Goat Anti-Rabbit (for ECE1) secondary antibodies (Vector Lab, 1:500) for 30 min. The slides were washed in PBS and then incubated with HRP-Streptavidin (Jackson Immunoresearch, 1:500) for 30 min and DAB Chromogen Substrate Solution (IHC World, 0.05% DAB) for 5–10 min and then washed with PBS and counterstained with Mayer's hematoxylin. The slide images were examined and documented under a microscope.

2.9. ECE1 enzymatic activity

ECE1 activity was determined using a fluorometric assay kit (K536-100) purchased from BioVision, Inc. (Milpitas, CA). Briefly, kidney samples (50 mg) were homogenized with an ice-cold buffer containing a protease inhibitor. Samples were centrifuged, and the supernatant was collected. The collected supernatants were diluted (1:5) with ECE1 assay

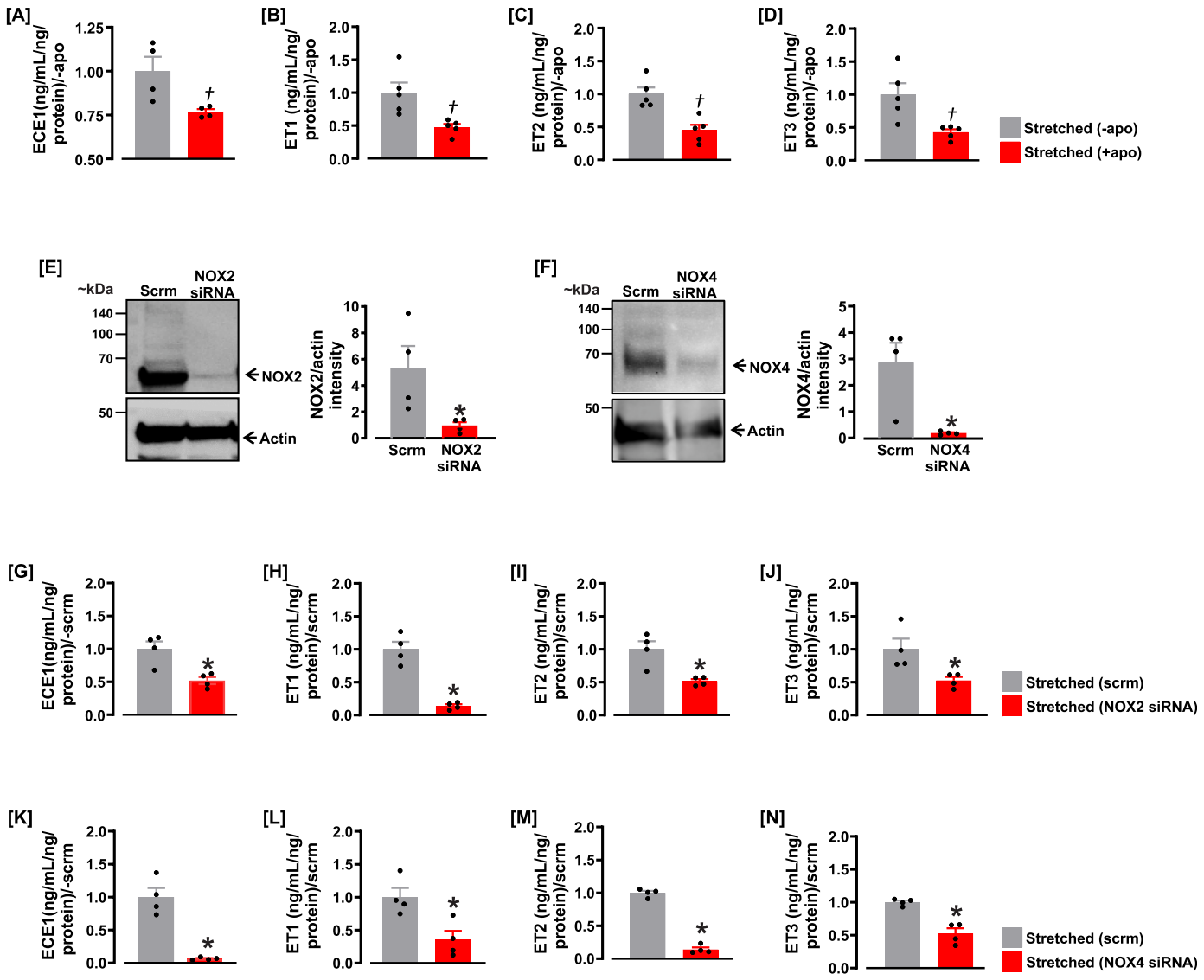

Fig. 4. Mechanical stretch-induced ECE1 and ET1-3 production in LLC-PK1 cells is dependent on NOX2 and NOX4. A-D, cellular ECE1, and ET1-3 in unstretched and stretched cells in the absence and presence of apocynin (apo; 20 μM). E and F, Representative Western blot demonstrating siRNA-mediated knockdown of NOX2 and NOX4. Cellular ECE1, and ET1-3 in cells transfected with scrambled (scrm; control) and NOX2 (G-J) and NOX4 (K-N) siRNA. $^{\dagger}P < 0.05$ vs. stretched (-apo); $^{*}P < 0.05$ vs. scrm (unpaired *t*-test).

buffer, and the fluorescence was measured (Ex/Em: 320/420 nm) in kinetic mode at 37 °C for 45 min. The assay was performed, and ECE1-specific activity was calculated according to the manufacturer's instructions.

2.10. Intracellular Ca^{2+} $[Ca^{2+}]_i$ imaging

$[Ca^{2+}]_i$ imaging was performed using a fluorescence photometry system (Ionoptix Corp., Milton, MA, USA) as we have described previously [41,49,51]. Briefly, afferent arterioles were isolated from sections of the kidney cortex in ice-cold modified Krebs' solution (MKS; 134 mM NaCl, 6 mM KCl, 2.0 mM $CaCl_2$, 2 mM $MgCl_2$, 10 mM HEPES, and 10 mM glucose, pH 7.4) under Zeiss SteREO Discovery.V12 stereomicroscope (Carl Zeiss, Thornwood, NY). The SMCs in the microvascular walls were loaded abluminally with Ca^{2+}-sensitive dye Fura-2-acetoxymethyl ester (Fura-2 AM; 10 μM) and 0.5% pluronic F-127 for ~ 1 h at room temperature in MKS [52]. The vessels were then immobilized in Cell-Tak (Corning Life Sciences, Corning, NY)-coated glass-bottom Petri dishes and washed for ~ 45 min to de-esterify the dye. Fura-2 AM was excited at wavelengths of 340 and 380 nm. Background-subtracted Fura-2 AM ratios were collected at 510 nm using a MyoCam-S CCD digital camera and analyzed with IonWizard software using the following equation [53]: $[Ca^{2+}]_i = K_d\ [(R - R_{min})/(R_{max} - R)]\ \delta$. Where "R" is the 340/380 nm ratio, R_{min} and R_{max} are the minima and maximum Fura-2 ratios determined in Ca^{2+}-free + EGTA and Ca^{2+}-replete solutions. δ represents the ratio of the 380 nm excitation in Ca^{2+}-free and Ca^{2+}-replete solution, while K_d is the apparent dissociation constant for Fura-2 (224 nM [53]). R_{min}, R_{max}, and δ were determined at the end of each experiment by perfusing the microvessels with 10 μM ionomycin and Ca^{2+}-free (plus 10 mM EGTA) or 10 mM Ca^{2+} solution.

2.11. Renal microcirculation measurement in reversible UUO

Newborn pigs were acutely instrumented with femoral artery and vein catheters, as we have previously described [47–50]. Total renal blood flow (tRBF), renal cortical perfusion, and mean arterial pressure (MAP) were recorded using a volume flowmeter (Transonic Systems Inc., Ithaca, NY), Laser-Doppler (Perimed, Jarfalla, Sweden), and

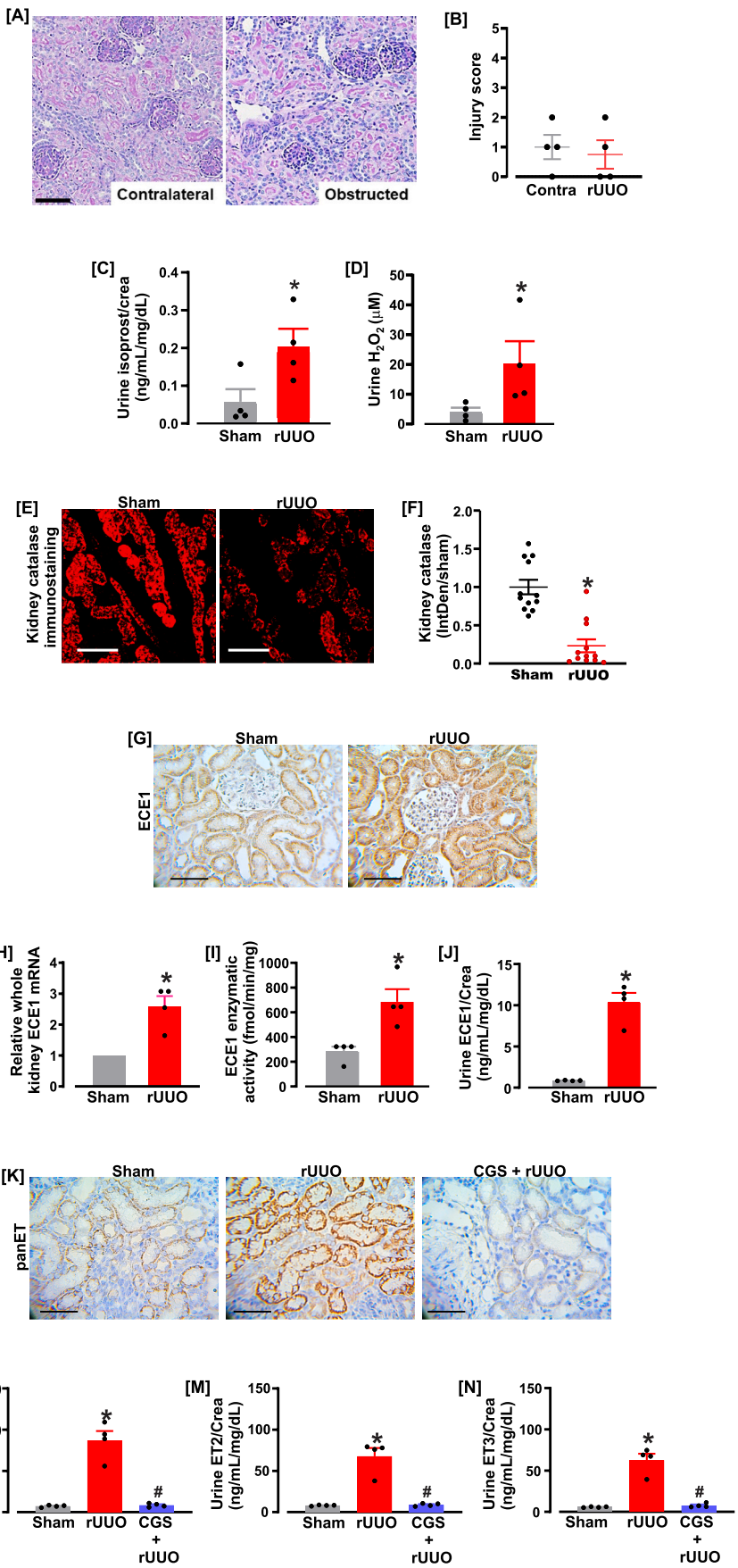

Fig. 5. Acute rUUO stimulated H_2O_2 generation and ECE1-dependent ET1-3 production in neonatal pig kidneys. A and B, kidney sections and morphological injury score in contralateral and obstructed kidneys. C and D, urinary isoprostane and H_2O_2 levels in sham- and rUUO- operated pigs. E and F: catalase immunostaining of sham and rUUO-operated kidney sections. G-J, kidney IHC (n = 4), mRNA expression levels, enzymatic activity, and urinary levels of ECE1 in sham and rUUO pigs. K–N, kidney IHC (n = 4) and urinary levels of ET in sham, rUUO, and CGS + rUUO pigs. *P < 0.05 vs. sham; #P < 0.05 vs. rUUO; [unpaired *t*-test (B-D, F, H-J); one-way ANOVA, with Holm-Sidak post hoc test (L–N)]. Scale bar = 50 μm.

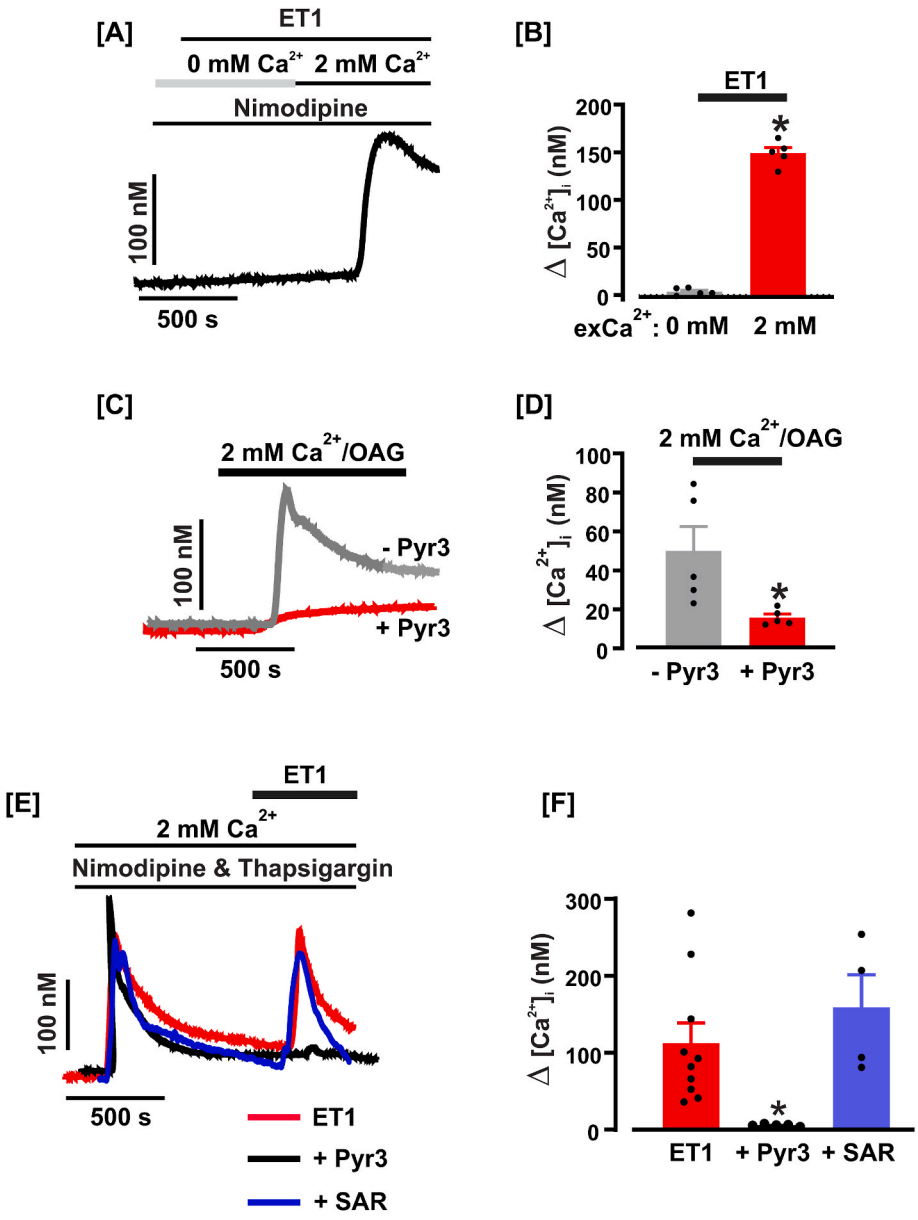

Fig. 6. Activation of ET_R stimulated ROCE in afferent arterioles A, representative tracings illustrating that ET1 (1 μM) did not alter $[Ca^{2+}]_i$ in neonatal pig afferent arteriole SMCs in the absence of extracellular Ca^{2+}. B, bar graphs summarizing $[Ca^{2+}]_i$ in ET1-treated neonatal pig afferent arterioles in the absence and presence of extracellular Ca^{2+}. C and D: tracings and graphs showing that OAG (10 μM)-induced $[Ca^{2+}]_i$ elevation in neonatal pig afferent arteriole SMC is dependent on TRPC3 channels. E and F, ET-1-induced $[Ca^{2+}]_i$ elevation in neonatal pig afferent arteriole SMC is independent of SR Ca^{2+}, unaltered by SAR (1 μM), but abolished by Pyr3 (1 μM); *P < 0.05 vs. 0 mM, Pyr3, and ET1 [unpaired *t*-test (B and D); one-way ANOVA, with Holm-Sidak post hoc test (F)].

physiological pressure transducer (ADInstruments, Colorado Spring, CO) systems, respectively [47–49]. All recordings were acquired simultaneously using the PowerLab data acquisition system and LabChart Pro software (ADInstruments, Colorado Spring, CO). To understand early renal hemodynamics changes caused by UUO-induced renal cell stretch without morphological injury, we subjected a group of neonatal pigs to 3 h of UUO by complete ligation of the ureter of the left kidney, after which the obstruction was removed, and the animals were allowed to recover for 3 h. The sham group was subjected to surgical procedures without ureteral ligation. A cohort of the piglets was administered pharmacological modulators via intrarenal arteries before UUO and during the recovery periods.

2.12. Western immunoblotting

Using RIPA lysis buffer, total proteins were isolated from pooled renal afferent arterioles and interlobular arteries per animal. After determination of concentration, the proteins were denatured using LDS sample buffer + DTT and heated at 70 °C for 10 min. Proteins were then separated on polyacrylamide gels in a Mini *Trans*-Blot Cell (Bio-Rad) and transferred onto PVDF membranes using a semi-dry blotter. The membranes were blocked for ~1 h using Tris Buffered Saline supplemented with 0.05% Tween (TBS-T) and 5% nonfat milk. The membranes were then incubated with respective primary antibodies overnight at 4 °C. After a wash in TBS-T, the membranes were incubated in HRP-conjugated secondary antibodies for 45 min at room temperature. Immunoreactive proteins were visualized using a chemiluminescent reagent.

2.13. siRNA transfection

Cells were transfected with custom-made target-specific porcine NOX2 and NOX4 siRNAs or a non-targeting scrambled (scrm) control siRNA (MilliporeSigma; Burlington, MA, USA) for 72 h using lipofectamine RNAiMAX transfection reagent (Life Technologies). Western immunoblotting was used to confirm knockdown efficiency.

2.14. Antibodies and reagents

Rat monoclonal anti-pan-ET (GeneTex, Irvine, CA; GTX40860),

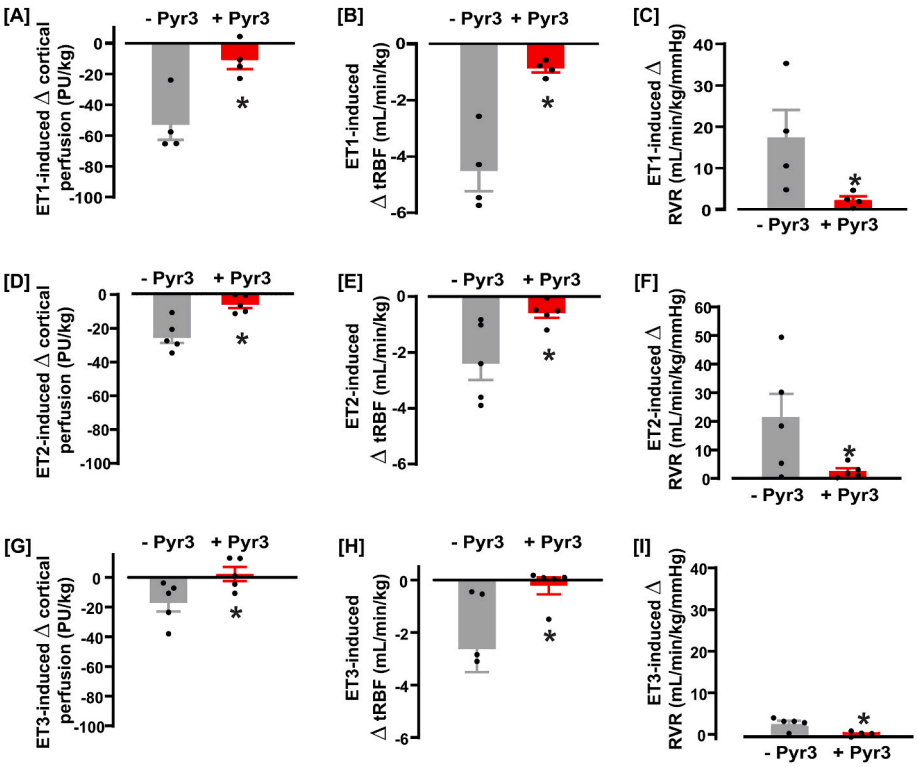

Fig. 7. ET caused hypoperfusion via TRPC3 channels in neonatal pigs. A-I, ET1-3 (10 ng/kg/min; 20 min) reduced kidney cortical perfusion and tRBF and increased RVR in neonatal pig, which Pyr3 pretreatment (1 μg/kg/min; 15 min) attenuated. *P < 0.05 vs. -Pyr3; (unpaired *t*-test).

rabbit polyclonal *anti*-ECE1 (Life Technologies, Grand Island, NY; PA5-81948), rabbit monoclonal anti-catalase (Abcam, Cambridge, MA; ab209211), rabbit monoclonal *anti*-NOX2 (Abcam; ab129068), rabbit monoclonal *anti*-NOX4 (Abcam; ab133303), rabbit polyclonal *anti*-TRPC3 (Alomone, Jerusalem Israel; ACC-016), rabbit polyclonal anti-ET receptor A (Alomone; AER-001), rabbit polyclonal anti-ET receptor B (Bioss Antibodies, Woburn, MA; bs-4198R), and mouse monoclonal anti-beta actin (Life Technologies; MA515739) were used. Secondary antibodies for Western blot (anti-mouse: 1:5000; anti-rabbit: 1:15000; Abcam) and immunofluorescence (CF488 Donkey anti-mouse and CF555 Donkey anti-Rabbit at 1:400 dilutions; Biotium, Inc, Fremont, CA) were used. Primary antibodies for Western blot and immunofluorescence were at 1:300 and 1:100 dilutions, respectively.

Unless specified, all reagents were purchased from MilliporeSigma (Burlington, MA). EUK 134 (EUK), ionomycin and bosentan (Cayman Chemical; Ann Arbor, MI), CGS 35066 (CGS), and SAR 7334 (SAR) (Tocris; Bristol, UK), apocynin, and thapsigargin (Life Technologies) were used.

2.15. Statistical analysis

Data are presented as mean ± standard error of the mean. The student's t-test and ANOVA, followed by the Holm-Sidak post hoc test, were used to compare unpaired and multiple tests (Graph Pad, Sacramento, CA). Statistical significance implies a P-value < 0.05.

3. Results

3.1. H_2O_2 generation induced ECE1-dependent ET1-3 production by LLC-PK1 cells

ECE1 and ET1 isoforms are predominantly expressed in LLC-PK1 cells and whole neonatal pig kidneys (Fig. 1). To investigate whether H_2O_2 stimulates ECE1 production in LLC-PK1 cells, sustained cellular H_2O_2 was generated using glucose oxidase (GO), an oxidoreductase that enzymatically derives H_2O_2 from β-D-glucose. As shown in Fig. 2A, 8 h of GO treatment increased cellular H_2O_2 production, which EUK, a superoxide dismutase and catalase mimetic, reversed. GO increased cellular ECE1 levels and immunostaining (Fig. 2B–D). GO also increased cellular ET1-3 levels and panET immunostaining in the cells (Fig. 2E–I). GO-induced increases in ET1-3 were reversed in cells pretreated with EUK and ECE1 inhibitor CGS (Fig. 2E–I).

3.2. Mechanical stretch generated H_2O_2 in LLC-PK1 cells and induced ECE1-dependent ET1-3 production

As demonstrated by f-actin immunostaining, stretched LLC-PK1 cells are more elongated than unstretched cells (Fig. 3A). qRT-PCR showed that NOX2 and NOX4 mRNAs were increased 4- and 2-folds, respectively, in stretched LLC-PK1 cells (Fig. 3B and C). Stretched cells showed a significant reduction in catalase immunostaining and increased cellular H_2O_2 (Fig. 3D–F). Stretch-induced increase in cellular H_2O_2 and ECE1 was reversed by EUK (Fig. 3 F and G). ET1-3 levels were also increased in the stretched cells, which EUK and CGS attenuated (Fig. 3H–J). NOX inhibitor apocynin diminished stretch-induced ECE1 and ET1-3 production (Fig. 4A–D). Furthermore, siRNA-mediated knockdown of NOX2 and NOX4 attenuated stretch-induced ECE1 and ET1-3 (Fig. 4E–N).

3.3. Acute reversible UUO stimulated H_2O_2 generation and ECE1-dependent ET1-3 production in neonatal pig kidneys

Obstructing the left ureter for 3 h, followed by 3 h of recovery, did not cause significant morphological kidney injury in neonatal pigs (Fig, 5 A and B). However, acute reversible UUO (rUUO) increased urinary isoprostane (renal oxidative stress marker) and H_2O_2 in the pigs (Fig. 5C and D). Immunostaining of catalase was also decreased in pigs' kidneys subjected to acute rUUO (Fig. 5E and F). IHC indicated the expression of ECE1 in the kidney tubules, which was amplified by rUUO (Fig. 5G). The mRNA expression, enzymatic activity in kidney tissues, and urinary

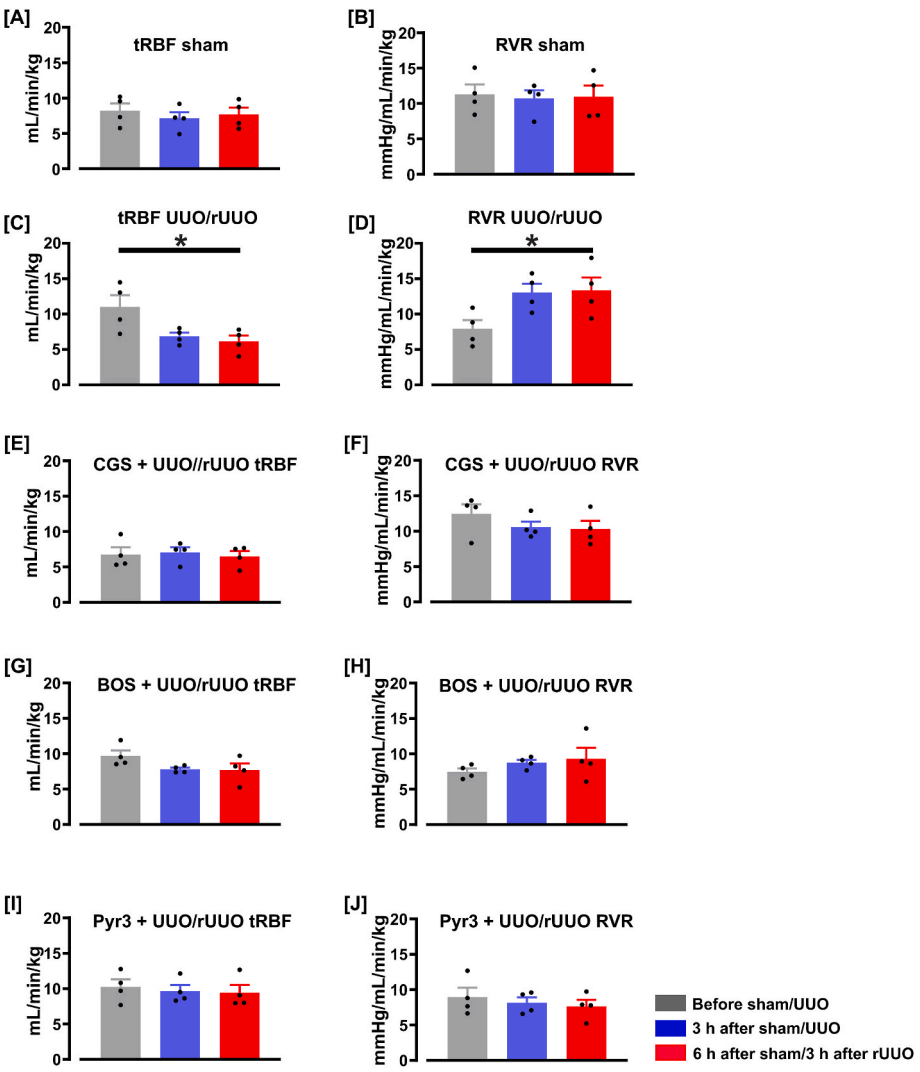

Fig. 8. rUUO caused persistent renal hypoperfusion in neonatal pigs via activation of ECE1/ET_R/TRPC3 signaling pathway. Bar graphs summarizing: A-J, tRBF and RVR in sham- and rUUO-operated neonatal pigs before sham or rUUO, 6 h after sham or 3 h after relief from UUO operations, and the effects of CGS (1 μg/kg/min; 30 min), bosentan (1 μg/kg/min; 30 min), and Pyr3 (1 μg/kg/min; 30 min) on rUUO. *P < 0.05 vs. before rUUO; (one-way ANOVA, with Holm-Sidak post hoc test).

levels of ECE1 after rUUO were higher than in sham-operated pigs (Fig. 5H–J). The renal tubular immunostaining and urinary levels of ET1-3 were increased in rUUO pigs, which CGS reversed (Fig. 5K-N).

3.4. Activation of ET receptors (ET_R) triggered receptor-operated Ca^{2+} entry (ROCE) in afferent arteriolar SMC and caused hypoperfusion via TRPC3 channels in neonatal pigs

In the absence of extracellular Ca^{2+}, ET did not increase $[Ca^{2+}]_i$ in neonatal pig afferent arterioles (Fig. 6A and B). Restoration of extracellular Ca^{2+} resulted in ET-induced increase in $[Ca^{2+}]_i$ by ~ 150 nM (Fig. 6 A and B). ROCE activator DAG analog OAG significantly increased $[Ca^{2+}]_i$ in the microvessels, which selective TRPC3 blocker Pyr3 attenuated (Fig. 6C and D). Despite blockade of L-type voltage-gated Ca^{2+} channels (LVGCC) with nimodipine and depletion of intracellular Ca^{2+} stores with thapsigargin, activation of ET_R was still able to increase $[Ca^{2+}]_i$ levels (Fig. 6E and F). Whereas selective TRPC6 channel blocker SAR 7334 had no effect, Pyr3 essentially abolished ET1-induced ROCE.

Infusion of ET1-3 directly into the kidneys to minimize their systemic effects resulted in a reduction in kidney cortical perfusion and tRBF and an increase in RVR, which were attenuated by Pyr3 (Fig. 7A–I).

3.5. rUUO caused renal hypoperfusion via activation of ECE1/ET_R/TRPC3

Fig. 8A and B show that tRBF and RVR in sham-operated pigs were unchanged. By contrast, tRBF was reduced, and RVR was increased during UUO and did not recover despite obstruction removal (Fig. 8C and D). Treatment of the pigs with CGS, ET_R antagonist bosentan, and pyr3 reversed the rUUO-induced reduction in tRBF and increase in RVR (Fig, 8 *E*-J).

3.6. rUUO did not alter protein expression levels of ET_R and TRPC3 but induced early AKI via activation of ECE1/ET_R/TRPC3 signaling

Western blot of proteins isolated from neonatal pig renal microvessels and probed with *anti*-ET_{RA}, ET_{RB}, and TRPC3 antibodies showed their expressions were unaltered in pigs subjected to acute rUUO (Fig. 9A–C). rUUO increased the urinary levels of early AKI biomarkers NGAL, L-FABP, and IL-18 (Fig. 9D–F). rUUO-induced increases in these biomarkers were overturned by CGS, bosentan, and Pyr3 (Fig. 9D–F).

4. Discussion

We show here that in neonatal pigs: *1)*, the mechanical stretch of PT

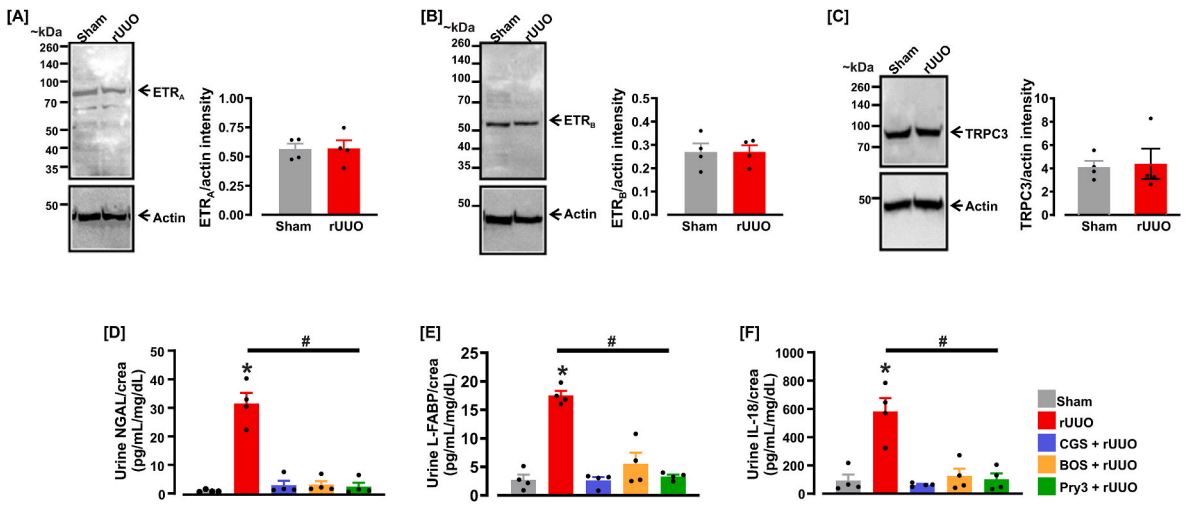

Fig. 9. rUUO did not alter protein expression levels of ET_R and TRPC3 but caused early AKI via activation of ECE1/ET_R/TRPC3. A-C, representative Western blot showing ET_{RA}, ET_{RB}, and TRPC3 protein expression in renal vessels of neonatal pigs subjected to sham and rUUO operations. ET_{RA} and ET_{RB} blots were stripped and re-probed for β-actin. D-F, urinary NGAL, L-FABP, and IL-18 in sham-, rUUO-, and CGS (1 μg/kg/min; 30 min) + rUUO-, bosentan (1 μg/kg/min; 30 min) + rUUO-, and Pyr3 (1 μg/kg/min; 30 min) + rUUO-operated neonatal pigs. Urinary NGAL, L-FABP, and IL-18 levels were normalized to urinary creatinine (crea). *$P < 0.05$ vs. sham; $^{\#}P < 0.05$ vs. rUUO; [unpaired *t*-test (A–C); one-way ANOVA, with Holm-Sidak post hoc test (D–F)].

epithelial cells stimulates H_2O_2, which triggers ECE1-dependent ET1-3 production; *2)*, NOX2 and NOX4 are sources of ROS-driven ET biosynthesis in the cells; *3)*, acute UUO, an inducer of tubular stretch and early renal ROS generation increased renal ET1-3, which is dependent on ECE1; *4)*, despite removing the obstruction, acute UUO caused kidney insufficiency in neonatal pigs characterized by a no-reflow phenomenon; *5)*, TRPC3-mediated Ca^{2+} signaling is an effector of ET-induced renal vasoconstriction; *6)*, although microvascular ET_R and TRPC3 protein expression are unaltered, inhibition of ECE1, ET_R, and TRPC3 attenuated rUUO-induced renal hypoperfusion and early AKI. These data suggest that UUO-engendered kidney tubular stretch drives ROS generation, stimulating ET biosynthesis and successive ET-induced activation of TRPC3-mediated persistent vasoconstriction and renal insufficiency.

The renal tubular epithelial cells are a primary ET source in the kidney [54]. Bioactive ET is derived from a 38 amino acid big ET by enzymatic cleavage at the Trp21-Va122 site by the action of ECE. We provide new data here indicating that ET1 and ECE1, the best-characterized ET and ECE isoforms are the most abundant in neonatal pig PT cell line and whole kidneys. NOX2 and NOX4 are significant sources of renal ROS and contribute to obstructive nephropathy [21,55–57]. Evidence suggests a bidirectional relationship between ROS and ET signaling, where on the one hand, NOX and oxidative stress can be stimulated by ET; on the other hand, NOX-derived ROS is a significant inducer of ET biosynthesis in various cell types [58,59]. In particular, H_2O_2 increases bovine aortic endothelial cell ECE1 levels [19]. Findings from this study indicate that H_2O_2 generation in neonatal pig renal epithelial cells also promotes ECE1-dependent production of all ET isoforms. Consistent with previous studies in other cardiovascular cells [23–26], the mechanical stretch of PT cells triggers ROS (H_2O_2) generation. ROS increases cellular ECE1, which drives functional ET production. An increase in NOX2 and NOX4 in stretched cells and inhibition of stretch-induced ECE1 and ET by apocynin and NOX knockdown suggest that NOX-derived ROS mediates stretch-induced ET biosynthesis.

Stretch of kidney tubules is a significant trigger of obstructive nephropathy [20]. The late detrimental consequence of uncorrected urinary tract obstruction is renal fibrosis. However, prior to the development of renal fibrosis, urinary tract obstruction-induced stretch of intrarenal cells promotes several mechanisms, including ROS generation [60]. Renal perfusion is impeded in UUO, which may not fully recover regardless of removing the obstruction [6–8]. This phenomenon, caused by pre-and post-glomerular vasoconstriction, is similar to the "no-reflow" occurrence when complete tissue perfusion is impaired despite relieving the initial cause of hypoperfusion [6–8]. Based on the findings that stretch stimulates ROS-dependent ET production in PT cells, we hypothesize that increased ET production and downstream ET-induced vasoregulation may underlie early persistent renal hypoperfusion in neonates. To investigate this, we subjected newborn pigs to short-term acute rUUO when significant morphological damage to the kidney was absent. Of note, RBF and RVR did not recover despite the removal of obstruction, suggesting kidney impairment characterized by persistent vasoconstriction. As expected, rUUO increased the level of renal ROS in the pigs. rUUO also increased ECE1 levels. Since ECE1 was increased in pigs subjected to rUUO, we anticipated that ET levels would also be increased. This hypothesis was supported by IHC staining demonstrating increased renal tubular ET, which was dependent on ECE1.

Almost all systemic plasma ET filtered in renal glomeruli is degraded within the kidney by endopeptidase and metalloendopeptidase [61–63]. Injection of radiolabelled ET1 into the systemic circulation also yielded an insignificant amount in the urine [64]. Thus, circulating ETs are not excreted in the urine, and urinary ETs are mainly of renal origin [61–64]. To confirm that amplified ET biosynthesis within the kidney contributes to hypoperfusion in neonatal UUO, we first used a porcine-specific ECE1, ET1-3 ELISA kits to measure their urinary levels in pigs subjected to rUUO. The urinary level of ECE1 in rUUO was ~12-fold higher compared with sham-operated pigs. Similarly, urinary ET1-3 levels were significantly elevated in rUUO-operated pigs. Remarkably, rUUO-induced increases in urinary ET1-3 were all abrogated by direct inhibition of renal ECE1. Taken together, these data suggest that rUUO stimulates ECE1-dependent ET production in the kidneys of neonatal pigs.

TRPC3 and TRPC6 share a significant amino acid identity and are gated by DAG [65,66], but TRPC3 selectively mediates ET-induced cerebral artery constriction [37]. Here, we demonstrate that, unlike ANG II [50], ET does not stimulate SOCE but increases ROCE in neonatal pig renal microvascular SMCs. Pyr3, a TRPC3 blocker, reversed ROCE in the microvessels. Unlike the TRPC6 blocker, Pyr3 abolished ET1-induced ROCE. Moreover, all ET peptides caused kidney hypoperfusion which Py3 reversed. Pharmacological inhibition of ECE1, ET_R, and TRPC3 attenuated rUUO-induced persistent hypoperfusion and RVR increase. Hence, ET-induced TRPC3 activation likely contributes to RBF decrease in neonatal pigs. Our data is consistent with previous findings indicating

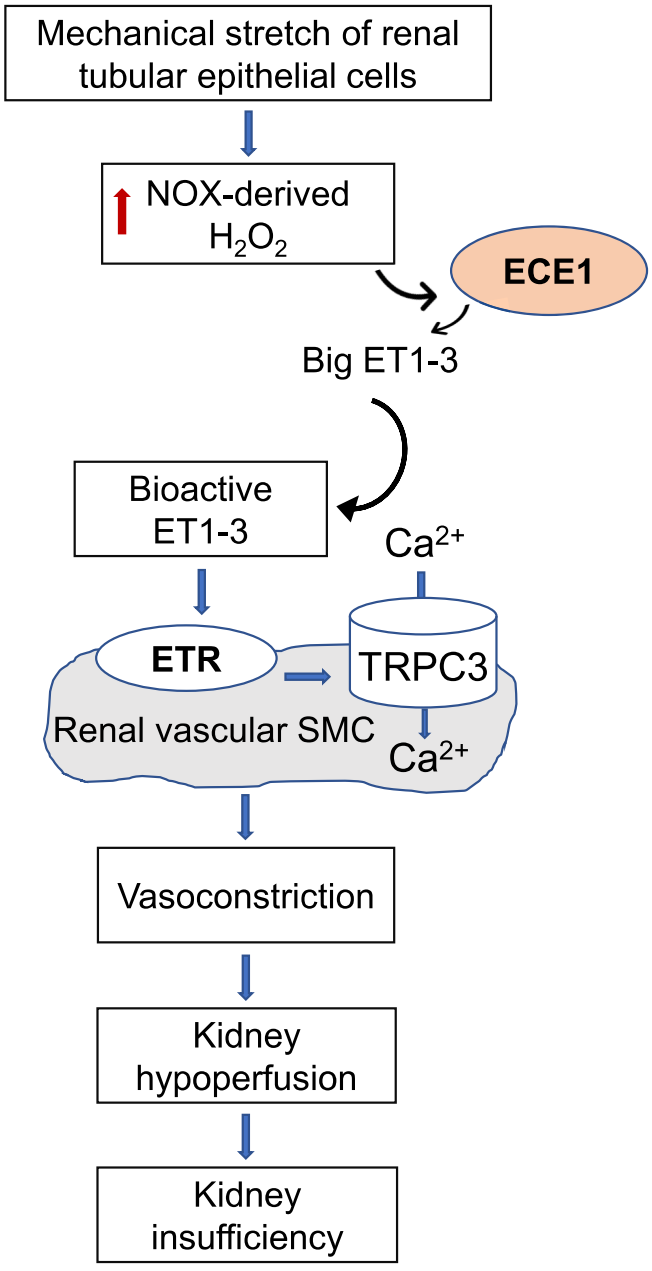

Fig. 10. The hypothetical pathway by which mechanical stretch impairs microcirculation and promotes early kidney insufficiency in neonatal pigs by inducing ROS-dependent biosynthesis of multiple ET isoforms and sequential activation of vascular SMC ET receptors and TRPC3 channels.

that ET_R inhibition attenuates UUO-induced decrease in rat RBF [11].

Western blot of protein lysates isolated from renal microvessels and probed with *anti*-ET_{RA}, ET_{RB}, and TRPC3 antibodies showed clear immunoreactive bands at ~75, 52, and 95 kDa, respectively. The predicted molecular weight of ET_{RA} is 48 kDa. ET_{RA} also shows glycosylated products between 66 and 123 kDa [67–70]. Hence, our experiments detected only the glycosylated ET_{RA}. ET_{RA}, ET_{RB}, and TRPC3 protein expression levels were unaltered in neonatal pigs subjected to rUUO, suggesting that acute rUUO-induced renal insufficiency in the pigs did not occur as a result of an increase in vascular ET_R or TRPC3. Since RBF was impaired by rUUO, we predicted early AKI in the pigs. Indeed, urinary NGAL, L-FABP, and IL-18, the early biomarkers of AKI, were increased in the pigs subjected to rUUO. These increases were reversed by ECE1, ET_R, and TRPC3 inhibitors, confirming that ECE1/ET_R/TRPC3 signaling is involved in rUUO-induced hemodynamic AKI (Fig. 10).

5. Conclusion

Although previous studies have demonstrated that urinary obstruction in neonates increased renal ET1 levels [9–12], much less is known about stretch-ET molecular links in obstructed kidneys. We provide novel data in this study suggesting that stretch-driven oxyradical generation stimulates the production of all ET isoforms in neonatal pig renal epithelial cells. ET activates renal vascular SMC TRPC3, leading to persistent vasoconstriction and RVR increase. These mechanisms may contribute to early vascular changes in neonatal AKI caused by urinary tract obstruction.

Funding

Dr. A. Adebiyi was supported by the National Institutes of Health under the award numbers R01DK101668, R56DK120595, R01DK120595, and R01DK127625. Dr. R. Kumar was supported by American Heart Association (AHA) Postdoctoral Fellowship 916180. The content of this publication is solely the authors' responsibility and does not necessarily represent the official views of the NIH and AHA.

Author contributions

Study conception and design: AA. Data acquisition and analysis: RK, HS, JMA, PK, PDM, SAI, and AA. Drafting of the manuscript: AA.

Declaration of competing interest

None.

Acknowledgment

We thank Robert Read, DVM, Ph.D., DAVCP (TriMetis Life Sciences, Memphis) for histological analysis.

References

[1] R.L. Chevalier, Perinatal obstructive nephropathy, Semin. Perinatol. 28 (2) (2004) 124–131.
[2] R.H. McLean, J.P. Gearhart, R. Jeffs, Neonatal obstructive uropathy, Pediatr. Nephrol. 2 (1) (1988) 48–55.
[3] K.S. Roth, H.P. Koo, S.E. Spottswood, J.C. Chan, Obstructive uropathy: an important cause of chronic renal failure in children, Clin. Pediatr. 41 (5) (2002) 309–314.
[4] N. Featherstone, S.A. Boddy, F.L. Murphy, Indications and relative renal function for paediatric nephrectomy over a 20-year period, Pediatr. Surg. Int. 27 (11) (2011) 1227–1231.
[5] J.P. Gaut, Nephrectomy for non-neoplastic kidney diseases, Surg Pathol. Clin. 7 (3) (2014) 307–319.
[6] N.J. Siegel, R.A. Feldman, B. Lytton, J.P. Hayslett, M. Kashgarian, Renal cortical blood flow distribution in obstructive nephropathy in rats, Circ. Res. 40 (4) (1977) 379–384.
[7] K. László, J. Juszkó, P. Bálint, Intrarenal haemodynamics in postobstructive diuresis in the dog, Acta Phys. Acad. Sci. Hungar. 53 (4) (1979) 409–425.
[8] W. Chaabane, F. Praddaude, M. Buleon, A. Jaafar, M. Vallet, P. Rischmann, C. I. Galarreta, R.L. Chevalier, I. Tack, Renal functional decline and glomerulotubular injury are arrested but not restored by release of unilateral ureteral obstruction (UUO), Am. J. Physiol. Ren. Physiol. 304 (4) (2013) F432–F439.
[9] H. Yanagisawa, K. Moridaira, O. Wada, Zinc deficiency further increases the enhanced expression of endothelin-1 in glomeruli of the obstructed kidney, Kidney Int. 58 (2) (2000) 575–586.
[10] S. Josephson, A. Hemsen, Renal tissue endothelin in long-term complete ureteric obstruction in the young rat, Urol. Int. 53 (2) (1994) 57–61.
[11] N.J. Hegarty, L.S. Young, A.J. O'Neill, R.W. Watson, J.M. Fitzpatrick, Endothelin in unilateral ureteral obstruction: vascular and cellular effects, J. Urol. 169 (2) (2003) 740–744.
[12] M.A. Taha, A.A. Shokeir, H.G. Osman, A. Abd el-Aziz Ael, S.E. Farahat, Diagnosis of ureteropelvic junction obstruction in children: role of endothelin-1 in voided urine, Urology 69 (3) (2007) 560–564. ; discussion 564-565.
[13] A. Inoue, M. Yanagisawa, S. Kimura, Y. Kasuya, T. Miyauchi, K. Goto, T. Masaki, The human endothelin family: three structurally and pharmacologically distinct

isopeptides predicted by three separate genes, Proc. Natl. Acad. Sci. U. S. A. 86 (8) (1989) 2863–2867.
[14] A.P. Davenport, K.A. Hyndman, N. Dhaun, C. Southan, D.E. Kohan, J.S. Pollock, D. M. Pollock, D.J. Webb, J.J. Maguire, Endothelin. *Pharmacol Rev* 68 (2) (2016) 357–418.
[15] A.C. Schroeder, J.D. Imig, E.A. LeBlanc, B.T. Pham, D.M. Pollock, E.W. Inscho, Endothelin-mediated calcium signaling in preglomerular smooth muscle cells, Hypertension 35 (1 Pt 2) (2000) 280–286.
[16] L. Ling, J.J. Maguire, A.P. Davenport, Endothelin-2, the forgotten isoform: emerging role in the cardiovascular system, ovarian development, immunology and cancer, Br. J. Pharmacol. 168 (2) (2013) 283–295.
[17] A.P. Davenport, R.E. Kuc, Cellular expression of isoforms of endothelin-converting enzyme-1 (ECE-1c, ECE-1b and ECE-1a) and endothelin-converting enzyme-2, J. Cardiovasc. Pharmacol. 36 (5 Suppl 1) (2000) S12–S14.
[18] C. Pupilli, P. Romagnani, L. Lasagni, F. Bellini, N. Misciglia, N. Emoto, M. Yanagisawa, M. Rizzo, M. Mannelli, M. Serio, Localization of endothelin-converting enzyme-1 in human kidney, Am. J. Physiol. 273 (5 Pt 2) (1997) F749–F756.
[19] S. Lopez-Ongil, M. Saura, C. Zaragoza, L. Gonzalez-Santiago, M. Rodriguez-Puyol, C.J. Lowenstein, D. Rodriguez-Puyol, Hydrogen peroxide regulation of bovine endothelin-converting enzyme-1, Free Radic. Biol. Med. 32 (5) (2002) 406–413.
[20] M.R. Quinlan, N.G. Docherty, R.W. Watson, J.M. Fitzpatrick, Exploring mechanisms involved in renal tubular sensing of mechanical stretch following ureteric obstruction, Am. J. Physiol. Ren. Physiol. 295 (1) (2008) F1–f11.
[21] A. Dendooven, D.A. Ishola Jr., T.Q. Nguyen, D.M. Van der Giezen, R.J. Kok, R. Goldschmeding, J.A. Joles, Oxidative stress in obstructive nephropathy, Int. J. Exp. Pathol. 92 (3) (2011) 202–210.
[22] J. Klein, J. Gonzalez, M. Miravete, C. Caubet, R. Chaaya, S. Decramer, F. Bandin, J. L. Bascands, B. Buffin-Meyer, J.P. Schanstra, Congenital ureteropelvic junction obstruction: human disease and animal models, Int. J. Exp. Pathol. 92 (3) (2011) 168–192.
[23] M.F. Montenegro, A. Valdivia, A. Smolensky, K. Verma, W.R. Taylor, A. San Martín, Nox4-dependent activation of cofilin mediates VSMC reorientation in response to cyclic stretching, Free Radic. Biol. Med. 85 (2015) 288–294.
[24] S. Wedgwood, S. Lakshminrusimha, P.T. Schumacker, R.H. Steinhorn, Cyclic stretch stimulates mitochondrial reactive oxygen species and Nox4 signaling in pulmonary artery smooth muscle cells, Am. J. Physiol. Lung Cell Mol. Physiol. 309 (2) (2015) L196–L203.
[25] C.W. Ward, B.L. Prosser, W.J. Lederer, Mechanical stretch-induced activation of ROS/RNS signaling in striated muscle, Antioxidants Redox Signal. 20 (6) (2014) 929–936.
[26] T. Girão-Silva, M.H. Fonseca-Alaniz, J.C. Ribeiro-Silva, J. Lee, N.P. Patil, L. A. Dallan, A.B. Baker, M.C. Harmsen, J.E. Krieger, A.A. Miyakawa, High stretch induces endothelial dysfunction accompanied by oxidative stress and actin remodeling in human saphenous vein endothelial cells, Sci. Rep. 11 (1) (2021), 13493.
[27] Z. Guan, J.P. VanBeusecum, E.W. Inscho, Endothelin and the renal microcirculation, Semin. Nephrol. 35 (2) (2015) 145–155.
[28] Y.H. Sandoval, M.E. Atef, L.O. Levesque, Y. Li, M.B. Anand-Srivastava, Endothelin-1 signaling in vascular physiology and pathophysiology, Curr. Vasc. Pharmacol. 12 (2) (2014) 202–214.
[29] D.M. Pollock, T.L. Keith, R.F. Highsmith, Endothelin receptors and calcium signaling, Faseb. J. 9 (12) (1995) 1196–1204.
[30] M.J. Berridge, Inositol trisphosphate and calcium signalling, Nature 361 (6410) (1993) 315–325.
[31] D. Narayanan, A. Adebiyi, J.H. Jaggar, Inositol trisphosphate receptors in smooth muscle cells, Am. J. Physiol. Heart Circ. Physiol. 302 (11) (2012) H2190–H2210.
[32] A.B. Parekh, J.W. Putney Jr., Store-operated calcium channels, Physiol. Rev. 85 (2) (2005) 757–810.
[33] J.W. Putney, Physiological mechanisms of TRPC activation, Pflügers Archiv 451 (1) (2005) 29–34.
[34] T. Gudermann, M. Mederos y Schnitzler, A. Dietrich, Receptor-operated cation entry–more than esoteric terminology? Sci. STKE 2004 (243) (2004) pe35.
[35] I. McFadzean, A. Gibson, The developing relationship between receptor-operated and store-operated calcium channels in smooth muscle, Br. J. Pharmacol. 135 (1) (2002) 1–13.
[36] C.S. Facemire, P.J. Mohler, W.J. Arendshorst, Expression and relative abundance of short transient receptor potential channels in the rat renal microcirculation, Am. J. Physiol. Ren. Physiol. 286 (3) (2004) F546–F551.
[37] A. Adebiyi, G. Zhao, D. Narayanan, C.M. Thomas-Gatewood, J.P. Bannister, J. H. Jaggar, Isoform-selective physical coupling of TRPC3 channels to IP_3 **receptors in smooth muscle cells regulates arterial contractility**, Circ. Res. 106 (10) (2010) 1603–1612.
[38] S.L. Archer, X.C. Wu, B. Thebaud, A. Nsair, S. Bonnet, B. Tyrrell, M.S. McMurtry, K. Hashimoto, G. Harry, E.D. Michelakis, Preferential expression and function of voltage-gated, O2-sensitive K+ channels in resistance pulmonary arteries explains regional heterogeneity in hypoxic pulmonary vasoconstriction: ionic diversity in smooth muscle cells, Circ. Res. 95 (3) (2004) 308–318.
[39] W.F. Jackson, E.M. Boerman, Regional heterogeneity in the mechanisms of myogenic tone in hamster arterioles, Am. J. Physiol. Heart Circ. Physiol. 313 (3) (2017) H667–h675.
[40] M.M. Khammy, J.A. Angus, C.E. Wright, Vascular reactivity of rabbit isolated renal and femoral resistance arteries in renal wrap hypertension, Eur. J. Pharmacol. 773 (2016) 32–41.
[41] H. Soni, D. Peixoto-Neves, R.K. Buddington, A. Adebiyi, Adenosine A1 receptor-operated calcium entry in renal afferent arterioles is dependent on postnatal maturation of TRPC3 channels, Am. J. Physiol. Ren. Physiol. 313 (6) (2017) F1216–f1222.
[42] P. Kanthakumar, A. Adebiyi, Renal vascular TRP channels, Curr Res Physiol 4 (2021) 17–23.
[43] S. Giraud, F. Favreau, N. Chatauret, R. Thuillier, S. Maiga, T. Hauet, Contribution of large pig for renal ischemia-reperfusion and transplantation studies: the preclinical model, J Biomed Biotechnol 2011 (2011), 532127.
[44] R. Reuter, Dellmann's Textbook of Veterinary Histology, sixth ed., Wiley-Blackwell, Hoboken, NJ, 2007.
[45] A. Eskild-Jensen, K. Thomsen, C. Rungø, L.S. Ferreira, L.F. Paulsen, Y. F. Rawashdeh, J.R. Nyengaard, S. Nielsen, J.C. Djurhuus, J. Frøkiaer, Glomerular and tubular function during AT1 receptor blockade in pigs with neonatal induced partial ureteropelvic obstruction, Am. J. Physiol. Ren. Physiol. 292 (3) (2007) F921–F929.
[46] A. Miyajima, J. Chen, D.P. Poppas, E.D. Vaughan Jr., Felsen D: **role of nitric oxide in renal tubular apoptosis of unilateral ureteral obstruction**, Kidney Int. 59 (4) (2001) 1290–1303.
[47] H. Soni, A. Adebiyi, Pressor and renal regional hemodynamic effects of urotensin II in neonatal pigs, J. Endocrinol. 217 (3) (2013) 317–326.
[48] H. Soni, A. Adebiyi, Early septic insult in neonatal pigs increases serum and urinary soluble Fas ligand and decreases kidney function without inducing significant renal apoptosis, Ren. Fail. 39 (1) (2017) 83–91.
[49] H. Soni, D. Peixoto-Neves, A.T. Matthews, A. Adebiyi, TRPV4 channels contribute to renal myogenic autoregulation in neonatal pigs, Am. J. Physiol. Ren. Physiol. 313 (5) (2017) F1136–f1148.
[50] H. Soni, D. Peixoto-Neves, M.A. Olushoga, A. Adebiyi, Pharmacological inhibition of TRPV4 channels protects against ischemia-reperfusion-induced renal insufficiency in neonatal pigs, Clin. Sci. (Lond.) 133 (9) (2019).
[51] A. Adebiyi, H. Soni, T.A. John, F. Yang, Lipid rafts are required for signal transduction by angiotensin II receptor type 1 in neonatal glomerular mesangial cells, Exp. Cell Res. 324 (1) (2014) 92–104.
[52] S.K. Fellner, W. Arendshorst, Endothelin-A and -B receptors, superoxide, and Ca^{2+} **signaling in afferent arterioles**, Am. J. Physiol. Ren. Physiol. 292 (1) (2007) F175–F184.
[53] G. Grynkiewicz, M. Poenie, R.Y. Tsien, A new generation of Ca^{2+} **indicators with greatly improved fluorescence properties**, J. Biol. Chem. 260 (6) (1985) 3440–3450.
[54] J.S. Speed, B.M. Fox, J.G. Johnston, D.M. Pollock, Endothelin and renal ion and water transport, Semin. Nephrol. 35 (2) (2015) 137–144.
[55] M. Sedeek, R. Nasrallah, R.M. Touyz, R.L. Hebert, NADPH oxidases, reactive oxygen species, and the kidney: friend and foe, J. Am. Soc. Nephrol. 24 (10) (2013) 1512–1518.
[56] C. Liu, Y. Song, L. Qu, J. Tang, L. Meng, Y. Wang, Involvement of NOX in the regulation of renal tubular expression of Na/K-ATPase in acute unilateral ureteral obstruction rats, Nephron 130 (1) (2015) 66–76.
[57] X. Qiao, L. Wang, Y. Wang, X. Su, Y. Qi, Y. Fan, Z. Peng, Intermedin inhibits unilateral ureteral obstruction-induced oxidative stress via NADPH oxidase Nox4 and cAMP-dependent mechanisms, Ren. Fail. 39 (1) (2017) 652–659.
[58] D.M. Pollock, J.S. Pollock, Endothelin and oxidative stress in the vascular system, Curr. Vasc. Pharmacol. 3 (4) (2005) 365–367.
[59] K.J. Dammanahalli, Z. Sun, Endothelins and NADPH oxidases in the cardiovascular system, Clin. Exp. Pharmacol. Physiol. 35 (1) (2008) 2–6.
[60] S. Washino, K. Hosohata, T. Miyagawa, Roles played by biomarkers of kidney injury in patients with upper urinary tract obstruction, Int. J. Mol. Sci. 21 (15) (2020).
[61] Z.A. Abassi, J.E. Tate, E. Golomb, H.R. Keiser, Role of neutral endopeptidase in the metabolism of endothelin, Hypertension 20 (1) (1992) 89–95.
[62] J. Janas, D. Sitkiewicz, A. Januszewicz, C. Szczesniak, R. Grenda, R.M. Janas, Endothelin-1 inactivating peptidase in the human kidney and urine, J. Hypertens. 18 (4) (2000) 475–483.
[63] Z.A. Abassi, H. Klein, E. Golomb, H.R. Keiser, Urinary endothelin: a possible biological marker of renal damage, Am. J. Hypertens. 6 (12) (1993) 1046–1054.
[64] A. Benigni, N. Perico, F. Gaspari, C. Zoja, L. Bellizzi, M. Gabanelli, G. Remuzzi, Increased renal endothelin production in rats with reduced renal mass, Am. J. Physiol. 260 (3 Pt 2) (1991) F331–F339.
[65] A. Dietrich, H. Kalwa, B.R. Rost, T. Gudermann, The diacylglycerol-sensitive TRPC3/6/7 subfamily of cation channels: functional characterization and physiological relevance, Pflügers Archiv 451 (1) (2005) 72–80.
[66] M. Trebak, G. Vazquez, G.S. Bird, J.W. Putney Jr., The TRPC3/6/7 subfamily of cation channels, Cell Calcium 33 (5–6) (2003) 451–461.
[67] D. Bousso-Mittler, R. Galron, M. Sokolovsky, Endothelin/sarafotoxin receptor heterogeneity: evidence for different glycosylation in receptors from different tissues, Biochem. Biophys. Res. Commun. 178 (3) (1991) 921–926.
[68] S. Tessier, S. Boivin, J. Aubin, P. Lampron, M. Detheux, A. Fournier, Transmembrane domain V of the endothelin-A receptor is a binding domain of ETA-selective TTA-386-derived photoprobes, Biochemistry 44 (21) (2005) 7844–7854.
[69] Z. Shraga-Levine, M. Sokolovsky, Functional role for glycosylated subtypes of rat endothelin receptors, Biochem. Biophys. Res. Commun. 246 (2) (1998) 495–500.
[70] D.E. Kohan, A.K. Hughes, S.L. Perkins, Characterization of endothelin receptors in the inner medullary collecting duct of the rat, J. Biol. Chem. 267 (17) (1992) 12336–12340.